JAAS

ROYAL SOCIETY OF CHEMISTRY

TECHNICAL NOTE

View Article Online
View Journal | View Issue

Cite this: *J. Anal. At. Spectrom.*, 2025, **40**, 1176

Nitrogen MICAP with post-plasma ionization mass spectrometry for elemental fluorine quantitation†

Jordan L. Tanen and Kaveh Jorabchi *

Recent developments in high-power nitrogen microwave plasmas have made them attractive excitation and ionization sources for elemental analysis, offering robust operation with liquid sample introduction and significant cost savings. However, nonmetal detection, particularly F analysis, remains challenging with these plasmas because of their lower excitation and ionization temperatures compared to Ar-ICP while the need for elemental F analysis continues to rise due to prevalence of fluorochemicals in pharmaceuticals and environmental contaminants. Here, we combine the advantages of a N_2 microwave inductively coupled atmospheric pressure plasma (MICAP) with those of post-plasma chemical ionization and evaluate the approach for elemental F analysis. The MICAP acts as a robust plasma reactor to break down fluorochemicals into HF which is then ionized to $ScFNO_3(H_2O)_n^+$ and detected by a quadrupole MS as ScF^+ after in-source ion activation. The approach offers a sensitivity of ~18 cps ng^{-1} mL of F, superior to < 4 cps ng^{-1} mL of F achieved by BaF^+ detection in Ar-ICP-MS/MS. An LOD of ~40 ng mL^{-1} of F is obtained comparable to those of Ar-ICP-MS/MS, limited by background equivalent concentration likely dominated by F contamination. F response factors are also independent of chemical species when sample introduction biases are minimized. However, broadening of flow injection peaks over time is observed, especially with high oxygen levels in the aerosol gas, denoting future areas of improvement for better analytical performance. These studies indicate a high potential of MICAP with post-plasma chemical ionization for F quantitation.

Received 14th February 2025
Accepted 11th April 2025

DOI: 10.1039/d5ja00059a

rsc.li/jaas

Introduction

Fluorochemicals are ubiquitous in the modern world with contributions to drug compounds,[1,2] pesticides,[3] and environmental contaminants (*e.g.* per- and polyfluoroalkyl substances),[4] necessitating development of analytical techniques for detecting and quantifying diverse species. Elemental F detection is particularly appealing in this regard, because of its capability for quantitation without compound-specific standards. As such, several studies have investigated inductively coupled plasma mass spectrometry (ICP-MS) for F detection.[5–9] A major obstacle in this area is poor ionization of F inside the ICP. F^+ formation is inefficient due to the high ionization potential of F, resulting in low detection sensitivity (0.03 cps ng^{-1} mL).[5] This has prompted efforts to use polyatomic ions formed inside the plasma to circumvent the high ionization potential of F, leading to identification of BaF^+ as an analytical ion with improved F detection sensitivities of 1.6–3.2 cps ng^{-1} mL.[6–8] One drawback of this approach is that BaF^+ formation is quite sensitive to plasma temperature at the ion sampling point as indicated by a narrow range of aerosol gas flow rates conducive to BaF^+ detection (1.3–1.4 L min^{-1}),[7,8] creating challenges for developing robust F detection methods.

Noting the challenges of in-plasma ionization, we have developed a post-plasma chemical ionization approach for F detection.[10–13] In contrast to ICP-MS, we use the plasma to convert F in fluorospecies to HF, which then undergoes atmospheric pressure chemical ionization downstream of the plasma by reagent ions produced from a nanospray ionization source. Interestingly, BaF^+ is also observed in this approach by using a Ba-containing electrolyte in nanospray, but with ~100 fold better sensitivity (281 cps ng^{-1} mL) compared to that in the ICP-MS studies.[10] The drastically improved ionization, however, is accompanied by susceptibility to interference from highly acidic species produced by the plasma.[11,12] In particular, nitric acid, abundantly generated when high levels of oxygen is added to the Ar-ICP to accommodate organic solvents, results in suppression of BaF^+ signal. Fortunately, the chemical tunability of the ionization reactions has resolved this limitation where using a Sc-containing electrolyte in nanospray results in formation of $ScFNO_3^+$ from gaseous HF in the presence of abundant nitric acid.[13] Further, large changes in aerosol flow rate (1.6–2.2 L min^{-1}) and RF power level (1100–1500 W) are found to have small effects on signal detection in this

Department of Chemistry, Georgetown University, Washington, DC 20057, USA. E-mail: kj256@georgetown.edu

† Electronic supplementary information (ESI) available. See DOI: https://doi.org/10.1039/d5ja00059a

approach,[14] highlighting minimal impact of plasma temperature on ion generation, thus affording more robust methods.

Moreover, thanks to the reduced effect of plasma properties on ion formation, a variety of plasma types can be readily coupled with post-plasma ionization for nonmetal detection. We have demonstrated F detection using dielectric barrier discharge coupled to chemical ionization[15] as well as P and S detection by polyatomic ion formation downstream of a solution cathode glow discharge.[16] Relatedly, recent years have seen a renewed interest in nitrogen plasmas for elemental analysis, partly fueled by high-power annular microwave plasmas that offer stable operation with solution introduction, high tolerance to organic solvents, and substantial savings in operating costs compared to Ar-ICP.[17–23] The compatibility with organic solvents is expected to facilitate coupling of gradient liquid chromatography to the plasma-based detectors. Notably, the N_2 microwave-sustained, inductively coupled, atmospheric-pressure plasma (MICAP) has also been adopted as an ionization source for elemental MS, showing promise in detection of metals and metalloids.[24–30] However, nonmetal detection with this ion source is yet to be achieved. Significantly lower excitation temperatures and Mg II/Mg I ratios in N_2-MICAP relative to those in Ar-ICP suggest a more difficult path for in-plasma ionization of nonmetals with this plasma.[31]

With the advantages noted above for N_2-MICAP regarding higher tolerance to organic solvents but lower ionization temperatures compared to Ar-ICP, we envisioned this plasma as a desirable reactor for nonmetal detection when coupled with post-plasma ionization. As such, this study describes the preliminary evaluation of N_2-MICAP to assess its potential for fluorine detection using post-plasma ionization and identifies areas of improvement. To our knowledge, this is the first effort in mass spectrometric elemental F analysis by using a nitrogen plasma.

Experimental

Sample preparation

The electrolyte solution for nanospray was prepared at 1 mM concentration in water purified to 18.2 MΩ cm (ELGA LabWater, Woodridge, IL) using scandium nitrate (Sigma-Aldrich, Milwaukee, WI). Fluorochemical samples were prepared from solid fluconazole, flucytosine, mefloquine hydrochloride, and *p*-fluoro-DL-phenylalanine (Sigma-Aldrich, Milwaukee, WI). Perfluoro-*n*-hexanoic acid, perfluoro-*n*-octanoic acid, perfluoro-*n*-decanoic acid were prepared by dilution from certified reference standards supplied at concentrations ~100 μg mL^{-1} in methanol (AccuStandard, New Haven, CT). All fluorochemical working solutions were prepared gravimetrically in 50 : 50 water : acetonitrile with 0.1% (v/v) formic acid to mimic solvent composition of a liquid chromatography experiment. The amount of methanol from certified reference standards in the final solutions was negligible.

Sample introduction, MICAP, and post-plasma ionization

Samples were injected using a PEEK flow injection loop size of 16 μL at solvent flow rate of 50 μL min^{-1}, delivered by a HPLC pump (1100 series, Agilent Technologies, Santa Clara, CA). 50 : 50 water : acetonitrile (Optima LC-MS grade, FisherScientific) with 0.1% (v/v) formic acid (Optima LC-MS grade, FisherScientific) was used as the solvent. The flow was aerosolized by a nebulizer (HEN-90, Meinhard, Golden, CO) into a cyclonic spray chamber (Meinhard, CO) using ultra-high purity nitrogen at a flow rate of 1.1 L min^{-1} and the aerosols were mixed with N_2 make-up gas using a tangential mixer (Meinhard, Golden, CO) prior to introduction into the torch. Aerosols were directed into the MICAP (Radom Instruments, Pewaukee, WI) through the 2.5 mm i.d. injector of a quartz torch (Meinhard, Golden, CO, model ML155023) whose outer tube protruded from the MICAP body by 2 mm.

The plasma sampling and downstream ionization were achieved by a homebuilt two-chamber interface schematically shown in Fig. 1. The design was similar to that reported previously.[13,14] A 3 mm nickel orifice (Spectron Inc, Ventura, CA), mounted on a cooled aluminum plate and placed 3 mm downstream of the torch, provided plasma sampling port while an exhaust flow installed above the torch outlet evacuated potentially harmful gases. Threaded aluminum rods connected the cooled aluminum plate and the MS (QTRAP, Sciex, Framingham, MA) ion sampling plate, sandwiching and tightly holding the two chambers.

The first chamber was composed of a 4.82 cm long, 5.08 cm o.d., 4.45 cm i.d. acrylic tube pressed between two aluminum disks and housed: (1) a quartz recombination tube (50 mm long 6.35 mm o.d. × 4 mm i.d.) with its entrance 5 mm downstream of the sampling orifice and fit to the left aluminum disk using graphite ferrule, (2) two parallel plate brass electrodes (10 mm × 10 mm × 3.17 mm), and (3) the nanospray ionization source. The second chamber was composed of a 20 mm long, 5.08 cm o.d., 4.45 cm i.d aluminum tube sandwiched between the middle aluminum disk and the ion sampling plate of the MS. A 5 mm L-shaped channel through the middle aluminum disk

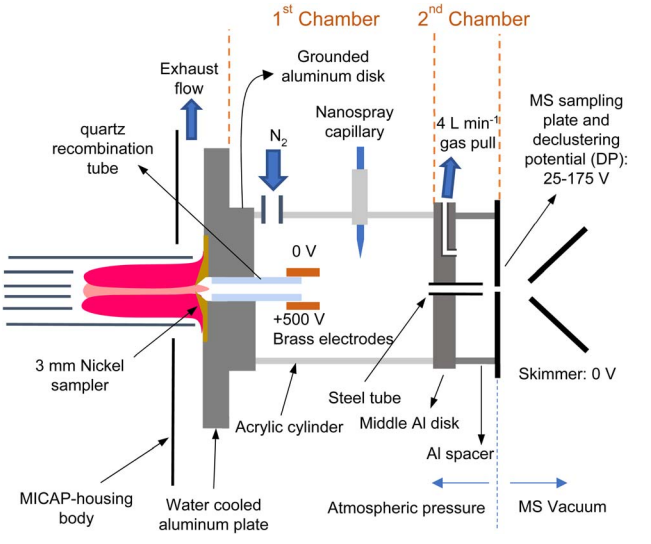

Fig. 1 Schematic of the N_2-MICAP coupled to post-plasma ionization interface. Figure reproduced with modifications from ref. 13.

allowed gas evacuation of the second chamber whose flow rate was monitored by a mass flow meter (Sierra Instruments, Monterey, CA). This evacuation pulled the gas from the first chamber toward the MS inlet through a steel tube (28 mm long, 4.5 mm i.d. × 6.35 mm o.d.) press fit into the middle aluminum disk. This arrangement mixed the ions generated by nanospray with neutrals generated by the plasma, enhancing ionization stability.

Plasma sampling was controlled by the flow rate of nitrogen into the first chamber (delivered by a mass flow controller, MKS instruments, Andover, MA) relative to the evacuation rate of the second chamber. The sampled plasma was cooled in the quartz tube, inducing recombination reactions to form HF from fluorochemicals introduced into the plasma.[11] The bottom brass electrode was biased to +500 V and the upper one was grounded to the MS to deflect ions and electrons coming from the plasma, minimizing plasma effects on nanospray operation while allowing plasma-generated neutral species to move toward the MS.

The plasma neutral products were ionized by reagent ions generated from a nanospray ionization source prepared from borosilicate capillaries (1 mm o.d., 0.75 mm i.d., WPI, Sarasota, FL) pulled to a diameter of ~5 μm with a micropipette puller (Sutter Instrument Company, Novato, CA, model P-87). The nanospray capillary was loaded with 1 mM scandium nitrate electrolyte and secured to a holder attached to the first chamber. The capillary protrusion was adjusted so that the spray tip was visually aligned with the top plane of the upper brass plate. A platinum electrode inserted into the capillary supplied the spray voltage (1300 to 1500 V). The nanospray-produced ions mixed with the plasma neutral products and were pulled toward the MS through the steel tube by the gas flow. The entrance of the steel tube was located 8 mm away from the nanospray tip, while its end was placed 4 mm upstream of the ion sampling plate of the MS. A fraction of the ions was sampled into the MS by the MS intake flow while the rest was swept away through the evacuation port of the 2nd chamber.

The operating parameters were optimized for best signal intensity *via* one factor at a time approach using flow injections of 1860 ng F mL^{-1} from fluconazole. Anticipating a minimal effect of plasma power based on our previous studies with Ar-ICP,[14] the gas flow optimizations were conducted at a middle power of 1300 W. Aerosol N_2 makeup gas of 0.4 L min^{-1} (yielding 1.5 L min^{-1} total aerosol gas flow rate) and torch coolant (outer) and auxiliary gas flow rates of 16 and 1.1 L min^{-1}, respectively, provided the optimized conditions for plasma operation. Although oxygen addition to aerosol gas is not required for preventing soot formation upon organic solvent introduction into N_2-MICAP, we noticed that small amounts of oxygen in aerosol gas improved the plasma stability (*e.g.* preventing sudden extinguishment) particularly at lower power levels. Given the minimal effect of power on signal generation, plasma operation at lower powers is preferred as it reduces the burden on interface cooling and minimizes energy usage. Therefore, 5 mL min^{-1} oxygen (controlled by a mass flowmeter, MKS instruments, Andover, MA) was added to 0.4 L min^{-1} N_2 makeup gas *via* a tee for all experiments, except for peak broadening studies where higher oxygen level was intentionally used to accelerate the broadening for more effective investigation. The interface gas evacuation flow rate was optimized at 4 L min^{-1} while 3.4–3.5 L min^{-1} interface N_2 input gas flow rate provided optimal F detection. The effect of power was checked in these conditions and in line with anticipation, no significant effect was observed in 1100–1500 W. The experiments were conducted at 1300 W unless otherwise noted.

MS operation

For background and reagent ion characterization, a low declustering potential (DP) of 25 V and a Q1 scan of *m*/*z* 20 to 500 with a scan time of 2 seconds were utilized. F-containing ions, also referred to as analytical ions, were detected by Q1 single ion monitoring of the ion of interest with a 500 ms dwell time. The details of analytical ion detection are further outlined in the next section.

Results and discussion

Sc-based reagent ions for post-MICAP chemical ionization of HF

F detection using post-plasma ionization is based on ionizing plasma-generated HF using metal-containing reagent ions supplied by nanospray where HF deprotonation is assisted by metal–F bond formation.[10,11,13] As noted in the introduction, abundant acidic plasma products, particularly those with high gas-phase acidity such as HNO_3, can interfere with these reactions.[11,13] Given the operation of MICAP with N_2, formation of such highly acidic plasma products is also anticipated. Importantly, such interferences can be avoided by selecting reagent ions with metals of high selectivity toward F^- relative to other anions. Our recent work in this area[13] identified Sc-based reagent ions for robust and sensitive HF detection in the presence of HNO_3 *via* reaction:

$$Sc(NO_3)_2(H_2O)^+_{n(g)} + HF_{(g)} \rightleftarrows ScNO_3F(H_2O)^+_{n(g)} + HNO_{3(g)} \quad (R1)$$

Accordingly, we selected Sc-based ionization for post-MICAP ionization of HF. To evaluate major MICAP products relevant to Sc-base ionization, we examined the ions generated from nanospray of a 1 mM Sc nitrate solution before and after interaction with plasma afterglow.

Fig. S1† depicts the effect of plasma sampling on nanospray ions. To monitor the original nanospray ions prior to any interaction with plasma afterglow, the plasma was kept off and the interface input nitrogen flow rate was set to 4.5 L min^{-1}. The higher input flow rate compared to the evacuation flow rate (4 L min^{-1}) ensures that the interface is flush with nitrogen (with extra gas pushing out of the sampling orifice) and that the lab air is prevented from entering the interface. Hydrated $Sc(OH)_2^+$, $Sc(OH)(NO_3)^+$, and $Sc(NO_3)_2^+$ are detected from nanospray (Fig. S1A†) in these conditions. These ions form during the electrospray ionization process, where nitrate ions bind to Sc^{3+} and hydroxide species are produced from hydrolysis by Sc(III).

When the plasma is turned on and the interface input nitrogen flow rate is lowered to 3.5 L min^{-1} to sample the

plasma into the interface, all Sc-containing ions convert into $Sc(NO_3)_2(H_2O)_n^+$, as depicted in Fig. S1B.† This conversion confirms abundant nitric acid formation in the plasma afterglow. No other major species are evident in Fig. S1B,† leaving $Sc(NO_3)_2(H_2O)_n^+$ as the main reagent ion for ionization of HF. With this confirmation, we proceeded to evaluate analytical performance for F detection *via* (R1) as discussed in the next section.

Analytical ion detection, linearity and LOD

To detect $ScFNO_3(H_2O)_n^+$ we initially utilized soft ion sampling (DP = 25) of the most abundant hydrate, $ScFNO_3(H_2O)_4^+$. However, similar to our previous studies, a need for fragmentation was evident to improve signal-to-background ratios, denoting presence of isobaric interferences. To minimize such interference and alleviate any issues with drifts in hydration levels of ions during experiments, we implemented a broad ion activation strategy. In this simple approach, a high declustering potential (175 V) is applied, fragmenting $ScNO_3F(H_2O)_n^+$ to ScF^+ during ion sampling from atmospheric pressure into the MS (also known as in-source fragmentation).

Analytical potential for F detection using ScF^+ was evaluated by constructing a calibration curve in the concentration range of 207–1881 ng mL^{-1} F using flow injection peak heights from injections of flucytosine as shown in Fig. 2. A linear regression model with weights of $1/\sigma_{signal}$ resulted in r^2 of 0.9988, indicating good linearity with a F sensitivity of 18.4 cps ng^{-1} mL. No detectable peaks were observed upon injections of blanks. A detection limit of 38 ng F mL^{-1} was determined based on $3 \times \sigma_{baseline}$/sensitivity where $\sigma_{baseline}$ was obtained from the standard deviation of the baseline prior to flow injections.

Notably, the sensitivity for F detection using MICAP with post-plasma nanospray ionization is substantially greater than those of ICP-MS methods utilizing in-plasma ion formation as

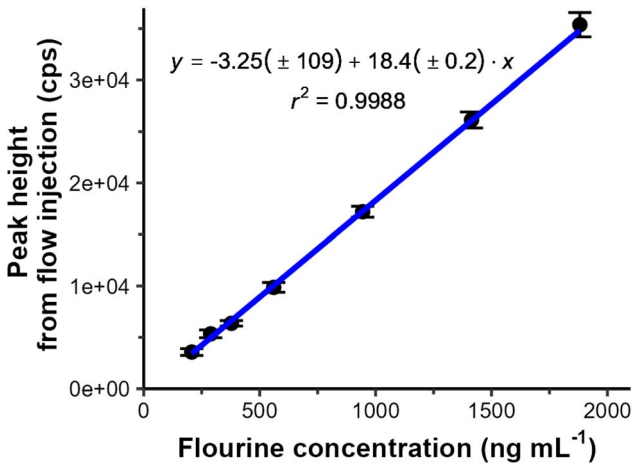

Fig. 2 ScF^+ signal calibration curve based on flucytosine flow injection peak heights. Error bars represent standard deviation from triplicate injections of sample. A linear model was constructed using weights of $1/\sigma_{signal}$, where σ_{signal} is the standard deviation of peak heights from triplicate injections. Experiments were performed with interface input nitrogen flow rate of 3.5 L min^{-1}.

Table 1 Comparison of analytical figures of merits between ICP-based mass spectrometric F detection techniques

Method	Ion or MS/MS transition	Integration time (ms)	LOD (ng mL^{-1})	BEC (ng mL^{-1})	Sensitivity (cps ng^{-1} mL)	Sample flow rate and solvent
ICP-HRMS[5]	F^+	N/A	5070	2050	0.026	100–150 µL min^{-1} water
ICP-MS/MS[7]	$BaF^+ \rightarrow BaF^+$	1000	43	607	3.2	330 µL min^{-1} water
ICP-MS/MS[6]	$BaF^+ \rightarrow BaF(NH_3)_3^+$	1000	22	21	1.6	300 µL min^{-1} water
ICP-MS/MS[8]	$BaF^+ \rightarrow BaF^+$	1000	60	400	2	Water (flow not reported)
ICP-MS[32]	BaF^+	9000	32	30	0.4	Water (flow not reported)
Ar-ICP-nanospray-MS[13]	$ScNO_3F(H_2O)_4^+$	500	19	357	360	50 µL min^{-1} 1 : 1 W : ACN
Ar-ICP-nanospray-MS/MS[13]	$ScNO_3F(H_2O)_4^+ \rightarrow ScFO_2^+$	500	16	120	14	50 µL min^{-1} 1 : 1 W : ACN
Ar-ICP-nanospray-MS/MS[14]	$ScNO_3F(H_2O)_4^+ \rightarrow ScFO_2^+$	500	2.2	25[a]	134[a]	50 µL min^{-1} 0.15 : 0.8 : 0.05 W : ACN : Ammonium hydroxide
N_2-MICAP-nanospray-MS (this work)	ScF^+ (broad ion activation)	500	38	437	18.4	50 µL min^{-1} 1 : 1 W : ACN

[a] Recalculated from original raw data obtained from author.

summarized in Table 1. The differences between sensitivities of various post-plasma ionization methods in Table 1 largely originate from variations in MS ion sampling and transmission efficiencies within different MS instruments as well as from differences in fragmentation schemes. Nonetheless, the sensitivity in the current work shows the potential of MICAP post-plasma ionization MS for F detection, particularly considering the use of a dated Qtrap MS platform.

The LOD for fluorine detection in the current work is within the range of LODs reported using ICP-MS/MS methods (20–60 ng F mL^{-1}). However, a higher LOD is obtained here compared to our previous works using post-ICP chemical ionization as noted in Table 1. This higher LOD is largely a result of higher background equivalent concentration (BEC) rather than major changes in signal stability. The BEC has contributions from isobaric interferences and F contamination. One potential isobaric interference is from $Sc^{18}OH^+$, as $ScOH^+$ is generated by in-source fragmentation of reagent ions, as shown in Fig. 3. Based on the isotopic distribution of $ScOH^+$, $Sc^{18}OH^+$ comprises about 2.9% of BEC, ruling out this ion as a major contributor. Further studies will be needed to confirm the components of BEC, however, based on our experience with Ar-ICPs coupled to high-resolution Orbitrap MS that readily separate isobaric interferences, we hypothesize F contamination from various sources is likely the major contributing factor to the BEC.

Compound-independent response

Noting the significance of species-independent response for quantitation of fluorochemicals, we evaluated this characteristic of MICAP with post-plasma ionization using 6 organofluorides with an array of chemical structures. Fig. 4A shows the response factors, defined as the flow injection peak area per ng mL^{-1} of F in injected sample. Five of the six compounds have response factors that lie within ±10% of their average, similar to species-independent response observed in other Ar-ICP-based post-plasma ionization studies.[10,14] However, perfluoro-*n*-octanoic acid (PFOA) behaves differently with 42% higher response factor than the average of the other 5 compounds.

To investigate the causes of this deviation, we considered potential sources of compound dependent response. Species-specific variation in response can arise from two processes: (1) differences in degradation of compounds inside the plasma, leading to HF production efficiency shifts, and (2) biases in sample introduction. While volatility is known to affect the analyte transport efficiency in sample introduction,[14] it is not clear if this effect is a major source for the deviation observed in Fig. 4A. The PFAS compounds are expected to have higher volatility but they do not show deviations consistent with their boiling points or vapor pressures (Table S1†). Nonetheless, the sample introduction biases can be minimized by using a high-transport efficiency setup (*e.g.* a single pass spray chamber), thus allowing the differentiation of the two causes noted above. To this end, we utilized a custom-built single pass spray chamber (~20 mL volume, Precision Glassblowing, Centennial, CO) with an orthogonal tangential makeup gas introduction port. The same HEN nebulizer was used but at a nebulizer N_2 gas flow rate of 0.4 L min^{-1} while makeup gases of 1.1 L min^{-1} nitrogen and 5 mL min^{-1} oxygen were added to maintain the same total aerosol flow rate and gas composition between the two spray chamber configurations. PFOA response factor was then measured along with that of *p*-fluoro-DL-phenylalanine. As depicted in Fig. 4B, about 2-fold higher response factor for the two compounds was measured using single pass spray chamber relative to those using cyclonic spray chamber, suggesting improved analyte transport efficiency. Further, the response factors for the two compounds were similar in Fig. 4B, denoting sample introduction bias as the main reason for deviation from species-independent response using cyclonic spray chamber. These studies show the importance of establishing species-independent response with new sample introduction configurations particularly when nebulizer gas is switched from typical argon gas.

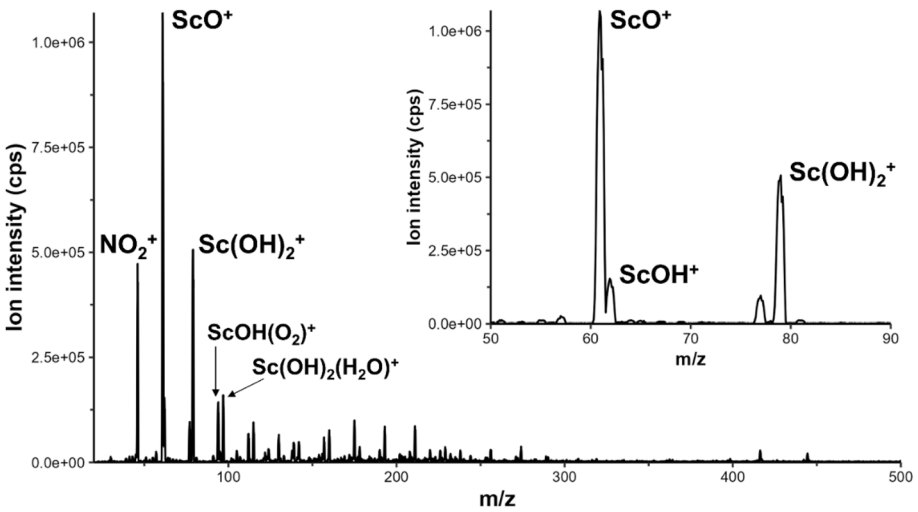

Fig. 3 Ions observed from in-source fragmentation (175 V DP) of reagent ions with plasma sampling (see Fig. S1B† with soft ion sampling for comparison). Experiments were performed with interface input nitrogen flow rate of 3.5 L min^{-1}.

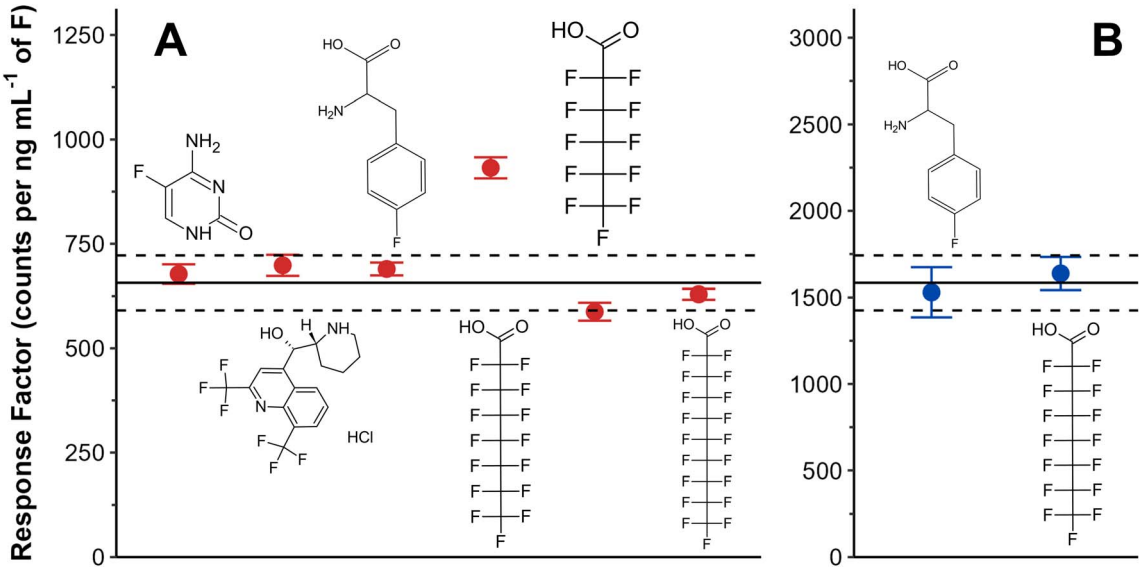

Fig. 4 (A) Response factors for 6 fluorinated compounds analyzed using a cyclonic spray chamber (red). From left to right: flucytosine, mefloquine hydrochloride, *p*-fluoro-DL-phenylalanine, perfluoro-*n*-octanoic acid, perfluoro-*n*-hexanoic acid, and perfluoro-*n*-decanoic acid. Straight line represents the average response factor for 5 compounds (excluding perfluoro-*n*-octanoic acid), with dashed lines representing the ±10% deviation window around the average response factor. (B) Response factors for 2 fluorinated compounds analyzed using a single pass spray chamber (blue). Straight line represent average between two compounds, with dashed lines representing ±10% deviation window. All tested compounds were prepared with F concentrations between 380 to 760 ng mL^{-1}. Nebulizer and makeup gas flow rates for single pass spray chamber were set to 0.4 and 1.1 L min^{-1} (+5 mL min^{-1} O_2), respectively.

Peak broadening

During the course of the above experiments, we noticed gradual broadening of flow injection peaks over time. To monitor peak broadening, we used the area-to-height ratio of flow injection peaks as a quantitative metric for peak shape. This metric describes an average duration of the transient signal. The theoretical lower limit can be calculated assuming a perfectly square peak, yielding 19.2 s width based on the injection loop volume and the solution flow rate. Over the course of 3 hours, we observed an increase in peak area-to-height ratio from ~30 to ~40 s. Broader peaks compromise chromatographic separations; thus, it is important to evaluate and resolve such broadening processes.

Notably, a major acceleration in peak broadening was observed when larger amounts of oxygen were introduced into the aerosol flow. On the other hand, using higher oxygen levels offered two advantages: (1) a more stable plasma operation at lower power levels, reducing burden on interface cooling and energy consumption without a compromise in ion generation efficiency; (2) maintaining an oxidative plasma chemistry and minimizing impact of solvent composition on end plasma products. The latter provides more robust post-plasma ionization and promotes full oxidation of carbon to CO_2, minimizing formation of toxic species such as HCN. With these considerations, the follow-up peak broadening investigations were conducted at 1100 W in accelerated broadening conditions by using 0.4 L min^{-1} oxygen (instead of nitrogen) as makeup gas merged with 1.1 L min^{-1} nitrogen aerosol gas from a cyclonic spray chamber.

Fig. 5A depicts the flow injection peaks in above conditions. A fresh quartz tube was used for these experiments. Peak broadening is visually observable in Fig. 5A starting at 20 minutes of plasma sampling time, defined as the amount of time elapsed since the interface nitrogen gas flow rate was lowered from 4.5 to 3.4 L min^{-1} to sample plasma into the interface. The area-to-height ratios of these peaks are shown by the red trace (Tube 1) in Fig. 5B, quantifying the broadening. Peak areas are plotted in Fig. 5C (red trace corresponding to Tube 1), showing constant signal response, confirming that no analyte was lost over time and that the change in area-to-height ratio was solely due to broadening.

Interestingly, when the post-plasma quartz tube was replaced with a fresh quartz tube, the behavior was reproduced with an initial narrow peak shape followed by broadening as shown in Fig. 5B (Tubes 2 and 3). The pace of broadening was variable between different tubes, however, they all produced similar peak areas (Fig. 5C). These observations suggest that plasma sampling modifies the surface of the quartz tube, leading to enhanced interactions of HF with the tube surface during passage to the ionization region. Interestingly, such high levels of peak broadening were not observed in our experiments using post-plasma chemical ionization with Ar-ICP,[10,13,14] denoting critical effect of plasma chemistry and plasma properties on recombination tube surface modification whose details remain to be elucidated. It is of note that eliminating high oxygen levels in the aerosol gas allows operation for several hours without significant peak broadening, enabling analytical measurements as reported in the earlier sections of this work.

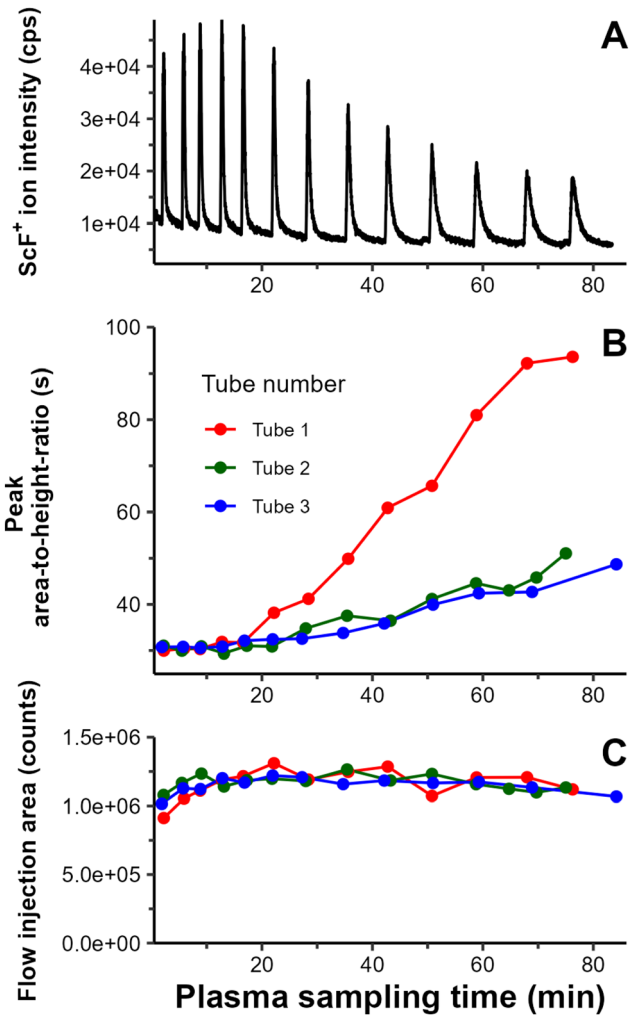

Fig. 5 (A) Flow injections of 1860 ng F mL^{-1} from fluconazole with a newly installed quartz tube. Plasma is sampled by lowering the interface nitrogen from 4.5 to 3.4 L min^{-1} at time zero. (B) Peak area-to-height ratios from injections of 1860 ng F mL^{-1} from fluconazole with three different freshly prepared quartz tubes. (C) Peak areas corresponding to injections in panel B. In all experiments, 0.4 L min^{-1} of oxygen was used as make-up gas with microwave power of 1100 W. All other parameters were the same as those denoted in Experimental section.

Conclusions

This study demonstrates the N_2-MICAP to be a viable plasma reactor for elemental F detection with post-plasma ionization. The N_2-MICAP is characterized as a nitric acid emitting plasma, requiring implementation of a Sc-based reagent ions to ionize plasma-produced HF. Using a simple in-source fragmentation method to create ScF^+ as analytical ion, a good signal linearity and better sensitivity compared to ICP-MS/MS methods are obtained with this approach. The detection limit is comparable to that of ICP-MS/MS methods, albeit improvements are expected upon reduction of BEC *via* elimination of F contamination. Elemental detection capabilities are further demonstrated by testing multiple fluorochemical compounds, showing species-independent response with one exception compound. The investigations suggested that biases in sample introduction rather than plasma chemistry in N_2-MICAP were responsible for deviation of this compound from ideal behavior, highlighting the need for characterization of sample introduction methods operated with alternative gases for species-independent quantitation. With a proper sample introduction method, deviations of less than 10% from average response are attainable with N_2-MICAP. As a point of comparison, the most frequently used total F quantitation method, combustion ion chromatography, shows far larger variations in response (66–110%),[33] further demonstrating the potential of MICAP with post-plasma ionization-MS for compound-independent F quantitation. The cost savings associated with nitrogen usage in MICAP relative to Ar-ICP further make this method desirable for F quantitation in high-throughput applications emerging in the PFAS quantitation arena.

Although quantitative potential is evident, peak broadening was observed throughout this study, particularly when high oxygen levels are used in the aerosol gas, degrading the performance over time. This effect is associated with adsorption/desorption of HF during passage through the quartz recombination tube. A redesign of the ionization interface to remove the quartz tube while maintaining plasma cooling for HF formation and effective chemical ionization would be a logical solution to eliminate the issue of peak broadening. The work in this area is underway in our laboratory.

Data availability

The data presented in this manuscript are provided in the ESI† within tabs of a .xlsx file.

Author contributions

Jordan L. Tanen: methodology, investigation, validation, formal analysis, writing-original draft, visualization, funding acquisition. Kaveh Jorabchi: conceptualization, methodology, writing-review and editing, supervision, project administration, funding acquisition.

Conflicts of interest

Kaveh Jorabchi is co-inventor on issued and pending patents related to the post-plasma chemical ionization technique investigated in this report.

Acknowledgements

This material is based upon work supported by the US National Science Foundation (NSF) under Grant CHE-1904835. Jordan Tanen is grateful for the Scholar Award from Achievement Rewards for College Scientists Foundation to enable acquisition of the MICAP unit used in this study. We thank Ashok Menon and Velibor Pikelja of Radom Instruments for their assistance in setting up and operating the MICAP unit.

References

1 M. Inoue, Y. Sumii and N. Shibata, Contribution of Organofluorine Compounds to Pharmaceuticals, *ACS Omega*, 2020, **5**, 10633–10640.
2 C. Zhang, Fluorine in Medicinal Chemistry: In Perspective to COVID-19, *ACS Omega*, 2022, **7**, 18206–18212.
3 P. Jeschke, in *Organofluorine Chemistry*, ed. K. Szabó and N. Selander, Wiley, 1st edn., 2021, pp. 363–395.
4 L. G. T. Gaines, Historical and current usage of per- and polyfluoroalkyl substances (PFAS): A literature review, *Am. J. Ind. Med.*, 2023, **66**, 353–378.
5 X. Bu, T. Wang and G. Hall, Determination of halogens in organic compounds by high resolution inductively coupled plasma mass spectrometry (HR-ICP-MS), *J. Anal. At. Spectrom.*, 2003, **18**, 1443–1451.
6 W. Guo, L. Jin, S. Hu and Q. Guo, Method Development for the Determination of Total Fluorine in Foods by Tandem Inductively Coupled Plasma Mass Spectrometry with a Mass-Shift Strategy, *J. Agric. Food Chem.*, 2017, **65**, 3406–3412.
7 N. L. A. Jamari, J. F. Dohmann, A. Raab, E. M. Krupp and J. Feldmann, Novel non-target analysis of fluorine compounds using ICPMS/MS and HPLC-ICPMS/MS, *J. Anal. At. Spectrom.*, 2017, **32**, 942–950.
8 Y. Zhu, K. Nakano and Y. Shikamori, Analysis of Fluorine in Drinking Water by ICP-QMS/QMS with an Octupole Reaction Cell, *Anal. Sci.*, 2017, **33**, 1279–1284.
9 N. L. A. Jamari, A. Behrens, A. Raab, E. M. Krupp and J. Feldmann, Plasma processes to detect fluorine with ICPMS/MS as [M–F] + : an argument for building a negative mode ICPMS/MS, *J. Anal. At. Spectrom.*, 2018, **33**, 1304–1309.
10 S. White, K. Zheng, J. Tanen, J. E. Lesniewski and K. Jorabchi, Elemental detection of fluorochemicals by nanospray-induced chemical ionization in afterglow of an inductively coupled plasma, *J. Anal. At. Spectrom.*, 2022, **37**, 870–882.
11 G. Hahm, F. A. Redeker and K. Jorabchi, Multielement Detection of Nonmetals by Barium-Based Post-ICP Chemical Ionization Coupled to Orbitrap-MS, *J. Am. Soc. Mass Spectrom.*, 2024, **35**, 871–882.
12 F. A. Redeker, J. E. Lesniewski, G. Hahm, W. P. McMahon and K. Jorabchi, High-Resolution Elemental Mass Spectrometry Using LC-ICP-Nanospray-Orbitrap for Simultaneous and Species-Independent Quantitation of Fluorinated and Chlorinated Compounds, *Anal. Chem.*, 2022, **94**, 11865–11872.
13 J. L. Tanen, S. R. White, D. Ha and K. Jorabchi, Fluorine-Selective Post-Plasma Chemical Ionization for Enhanced Elemental Detection of Fluorochemicals, *J. Anal. At. Spectrom.*, 2023, **38**, 854–864.
14 S. White and K. Jorabchi, Post-ICP Chemical Ionization MS for Total Extractable Organic Fluorine Quantitation, *ACS Omega*, 2024, **9**, 46634–46642.
15 K. Zheng, J. E. Lesniewski, M. J. Dolan, W. Li, T. T. Metallo and K. Jorabchi, Elemental Fluorine Detection by Dielectric Barrier Discharge Coupled to Nanoelectrospray Ionization Mass Spectrometry for Nontargeted Analysis of Fluorinated Compounds, *Anal. Chem.*, 2020, **92**, 10129–10137.
16 F. A. Redeker, K. O'Malley, W. P. McMahon and K. Jorabchi, Solution cathode glow discharge coupled to atmospheric pressure chemical ionization for elemental detection of S and P in organic compounds, *Spectrochim. Acta, Part B*, 2024, **212**, 106858.
17 M. R. Hammer, A magnetically excited microwave plasma source for atomic emission spectroscopy with performance approaching that of the inductively coupled plasma, *Spectrochim. Acta, Part B*, 2008, **63**, 456–464.
18 A. Akhdhar, M. Schneider, S. Hellmann, A. Orme, E. Carasek, E. M. Krupp and J. Feldmann, The use of microwave-induced plasma optical emission spectrometry for fluorine determination and its application to tea infusions, *Talanta*, 2021, **227**, 122190.
19 B. M. Fontoura, F. C. Jofré, T. Williams, M. Savio, G. L. Donati and J. A. Nóbrega, Is MIP-OES a suitable alternative to ICP-OES for trace element analysis?, *J. Anal. At. Spectrom.*, 2022, **37**, 966–984.
20 A. J. Schwartz, Y. Cheung, J. Jevtic, V. Pikelja, A. Menon, S. J. Ray and G. M. Hieftje, New inductively coupled plasma for atomic spectrometry: the microwave-sustained, inductively coupled, atmospheric-pressure plasma (MICAP), *J. Anal. At. Spectrom.*, 2016, **31**, 440–449.
21 H. Wiltsche and M. Wolfgang, Merits of microwave plasmas for optical emission spectrometry – characterization of an axially viewed microwave-sustained, inductively coupled, atmospheric-pressure plasma (MICAP), *J. Anal. At. Spectrom.*, 2020, **35**, 2369–2377.
22 O. V. Pelipasov and E. V. Polyakova, Matrix effects in atmospheric pressure nitrogen microwave induced plasma optical emission spectrometry, *J. Anal. At. Spectrom.*, 2020, **35**, 1389–1394.
23 R. Serrano, G. Grindlay, L. Gras and J. Mora, Microwave-sustained inductively coupled atmospheric-pressure plasma (MICAP) for the elemental analysis of complex matrix samples, *Talanta*, 2024, **271**, 125666.
24 M. Schild, A. Gundlach-Graham, A. Menon, J. Jevtic, V. Pikelja, M. Tanner, B. Hattendorf and D. Günther, Replacing the Argon ICP: Nitrogen Microwave Inductively Coupled Atmospheric-Pressure Plasma (MICAP) for Mass Spectrometry, *Anal. Chem.*, 2018, **90**, 13443–13450.
25 Z. You, A. Akkuş, W. Weisheit, T. Giray, S. Penk, S. Buttler, S. Recknagel and C. Abad, Multielement analysis in soils using nitrogen microwave inductively coupled atmospheric-pressure plasma mass spectrometry, *J. Anal. At. Spectrom.*, 2022, **37**, 2556–2562.
26 M. Kuonen, G. Niu, B. Hattendorf and D. Günther, Characterizing a nitrogen microwave inductively coupled atmospheric-pressure plasma ion source for element mass spectrometry, *J. Anal. At. Spectrom.*, 2023, **38**, 758–765.
27 M. Kuonen, B. Hattendorf and D. Günther, Quantification capabilities of N_2 MICAP-MS with solution nebulization and aerosol desolvation, *J. Anal. At. Spectrom.*, 2024, **39**, 1388–1397.

28 S. Mukta and A. Gundlach-Graham, Ion chromatography – nitrogen-sustained microwave inductively coupled atmospheric pressure plasma – mass spectrometry (IC-MICAP-MS) for arsenic speciation analysis in rice, *J. Anal. At. Spectrom.*, 2024, **39**, 491–499.

29 A. Winckelmann, J. Roik, S. Recknagel, C. Abad and Z. You, Investigation of matrix effects in nitrogen microwave inductively coupled atmospheric-pressure plasma mass spectrometry (MICAP-MS) for trace element analysis in steels, *J. Anal. At. Spectrom.*, 2023, **38**, 1253–1260.

30 Z. You, A. Winckelmann, J. Vogl, S. Recknagel and C. Abad, Determination of calcium, iron, and selenium in human serum by isotope dilution analysis using nitrogen microwave inductively coupled atmospheric pressure plasma mass spectrometry (MICAP-MS), *Anal. Bioanal. Chem.*, 2024, **416**, 3117–3125.

31 K. M. Thaler, A. J. Schwartz, C. Haisch, R. Niessner and G. M. Hieftje, Preliminary survey of matrix effects in the Microwave-sustained, Inductively Coupled Atmospheric-pressure Plasma (MICAP), *Talanta*, 2018, **180**, 25–31.

32 W. Guo, X. Lin, L. Jin and S. Hu, Single quadrupole inductively coupled plasma-mass spectrometry for the measurement of fluorine in tea infusions and its health risk assessment, *J. Food Compos. Anal.*, 2020, **86**, 103378.

33 R. Aro, U. Eriksson, A. Kärrman, I. Reber and L. W. Y. Yeung, Combustion ion chromatography for extractable organofluorine analysis, *iScience*, 2021, **24**, 102968.

